IOP Publishing Journal of Physics: Condensed Matter

J. Phys.: Condens. Matter **22** (2010) 104105 (12pp) doi:10.1088/0953-8984/22/10/104105

Self-assembly scenarios of patchy colloidal particles in two dimensions

Günther Doppelbauer[1], Emanuela Bianchi[1,2] and Gerhard Kahl[1]

[1] Institut für Theoretische Physik and Center for Computational Materials Science (CMS), Technische Universität Wien, Wiedner Hauptstraße 8-10, A-1040 Wien, Austria
[2] Erwin Schrödinger International Institute for Mathematical Physics, Boltzmanngasse 9, A-1090 Wien, Austria

E-mail: doppelbauer@cmt.tuwien.ac.at

Received 5 October 2009, in final form 5 November 2009
Published 23 February 2010
Online at stacks.iop.org/JPhysCM/22/104105

Abstract
We have investigated the self-assembly scenario of patchy colloidal particles in a two-dimensional system. The energetically most favourable ordered particle arrangements have been identified via an optimization tool that is based on genetic algorithms. Assuming different simple models for patchy colloidal particles, which include binary mixtures as well as attraction and repulsion between the patches, we could identify a broad variety of highly non-trivial ordered structures. The strategies of the systems to self-assemble become evident from a systematic variation of the pressure: (i) saturation of patch bonds at low pressure and close packing at high pressure and (ii) for intermediate pressure values, the strategy is governed by a trade-off between these two energetic aspects. The present study is yet another demonstration of the efficiency and the high reliability of genetic algorithms as versatile optimization tools.

(Some figures in this article are in colour only in the electronic version)

1. Introduction

In recent times, so-called patchy colloidal particles have attracted a considerable amount of interest in soft matter physics. Patchy particles are complex colloids whose basic features are the anisotropy in their interparticle interaction and their limited valence in bonding. From the experimental point of view, impressive progress has been made recently in synthesizing such colloids: particles with anisotropic shape as well as anisotropic interactions are beginning to be engineered at nanometre and micrometre scales. Indeed, a number of useful methods have been developed for the production of non-spherical colloids as monodisperse samples in relatively large quantities [1, 2]. Depending on the method, these colloids can be ellipsoidal, rod-shaped, polygonal and polyhedral [3–5]. One promising way of introducing selectivity and directionality in the interparticle interaction is chemical or physical patterning of the particle surfaces. For instance, these complex colloids can be obtained by coating non-additive spherically symmetric interacting particles with biological ligands that exhibit selective molecular recognition. This method of structural encoding is exceptionally powerful because of the wide variety of proteins, DNA and RNA that have a specific affinity for each other [6–14]. In all cases, patches are discrete and limited in number, thus ensuring a low coordination number of aggregation. Due to the specific shape of the particles and the asymmetric, selective and directional interactions, it will be possible to self-assemble these new complex colloids into predictable, precise, ordered structures. The new features of these novel building blocks could profoundly expand the range of self-assembled structures in colloidal science: the formation of rings, chains, sheets, icosahedra, square pyramids and tetrahedra has been shown to occur upon a suitable design of the patches pattern [15–18].

From the theoretical point of view, patchy models have been reintroduced recently, after they had been first investigated in the context of associating fluids in the 1980s (see, e.g., [19–23]). While in these original models the patches were parametrized as spot-like interactions, it has turned out that, in particular in soft and bio-related systems, it is more appropriate to consider rather extended (attractive) regions than spot-like interactions [24–26]. Two examples for this type of patchy colloids are realized in the Sear [27] or in the Kern–Frenkel [28] model. Based on computer simulations and theoretical approaches a deeper understanding has been achieved in a variety of phenomena: among those are

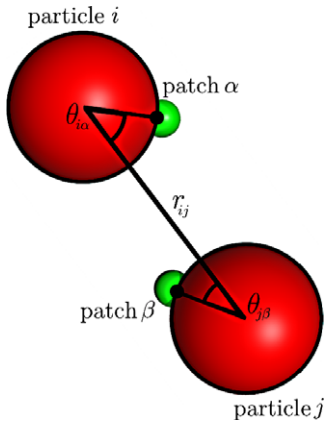

Figure 1. Schematic representation of two interacting patchy particles, introducing the parameters of the interparticle potential (cf equations (1)–(3)).

gelation [29–34], gas–liquid phase separation [35–37], fluid–fluid and sol–gel transitions [28, 38–40], or linear chains and network formation [41–43], to name a few.

While all these investigations were dedicated to the disordered phases, little has been achieved for the ordered phases: a few theoretical studies [18, 44–47] provide evidence that the features of selectivity and directionality of the patchy particle interactions are able to lead to a large variety of ordered structures, comprising both isolated clusters as well as ordered lattices. In some cases these self-assembly scenarios can be easily predicted by simply optimizing the saturation of patches (which holds in particular in two dimensions). However, the situation becomes more difficult when the model is extended, for instance, by proceeding to three dimensions, by introducing attraction and repulsion among the patches or by considering mixtures of patchy particles. Then it is highly non-trivial to predict and/or to identify all ordered equilibrium structures (or minimum energy configurations—MECs).

The aim of the present contribution is to introduce optimization techniques based on genetic algorithms (GAs) as a highly reliable and efficient tool to identify ordered equilibrium structures of patchy colloidal systems. Indeed, for a large variety of soft matter systems these tools have been successfully applied to identify ordered structures [48–65]. Most of them are based on a genotype implementation of the algorithm [66]. Here we apply GA-based optimization strategies *for the first time* to investigate MECs of patchy systems. In an effort to assess the reliability of the approach we restrict ourselves to rather simple models, keeping thereby the number of parameters low: we work in two dimensions and use a simple model for patchy particles that is closely related to the one introduced in [44]. Three different systems are considered: (i) patchy particles with purely attractive patches, testing thereby, in direct comparison with results presented in [44], the reliability of our approach; (ii) a binary mixture of patchy particles with attractive patches where the two components are characterized by different numbers of patchy sites and (iii) patchy particles that are decorated with attractive and repulsive patches.

In these investigations we have used a phenotype implementation of a GA-based optimization tool [67–71] in the NPT ensemble. Results can be summarized as follows: (i) for the one-component system with the attractive patches we could confirm most of the MECs identified in [44]; however, for a few cases we could also show that the GA-based tool is able to identify MECs that are energetically even more favourable and (ii) for the other two systems introduced above we could identify highly complex self-assembly scenarios; in addition, we are able to provide a deeper insight into the mechanisms of how the system self-assembles with increasing pressure.

This paper is organized as follows: in the subsequent section we briefly discuss the underlying model for the patchy particles and outline our implementation of the GA-based optimization tool. In section 3 we thoroughly discuss the results for the three different classes of systems mentioned above and close the paper with concluding remarks and an outlook on future work.

2. Model and theoretical tools

2.1. The model

The potential for our two-dimensional patchy colloidal system has been proposed in [44]. It consists, on the one hand, of an isotropic Lennard-Jones (LJ) potential:

$$V_{\mathrm{LJ}}(r) = 4\epsilon\left[\left(\frac{\sigma}{r}\right)^{12} - \left(\frac{\sigma}{r}\right)^{6}\right], \tag{1}$$

where σ and ϵ are used as length and energy units. In addition, an orientational dependence is introduced which characterizes the patches on the surface of the colloidal particles; this contribution is introduced via a modulating factor, $V_{\mathrm{ang}}(\mathbf{r}_{ij}, \mathbf{p}_{i\alpha}, \mathbf{p}_{j\beta})$, which is given by

$$V_{\mathrm{ang}}(\mathbf{r}_{ij}, \mathbf{p}_{i\alpha}, \mathbf{p}_{j\beta}) = \exp\left[-(\Theta_{i\alpha}^2 + \Theta_{j\beta}^2)/w^2\right]. \tag{2}$$

Here, $\mathbf{r}_{ij} = \mathbf{r}_i - \mathbf{r}_j$ is the vector between particles i and j, the patch vector, $\mathbf{p}_{i\alpha}$, specifies patch α of particle i, $\Theta_{i\alpha}$ is the angle between $\mathbf{r}_{ij}$ and $\mathbf{p}_{i\alpha}$; w specifies the extent of the patch along the circumference (see figure 1). If not otherwise stated, $w = 2\pi \cdot 0.05$. In total, the functional form of the potential is

$$V(\mathbf{r}_{ij}, \mathbf{p}_{i\alpha}, \mathbf{p}_{j\beta}) = \begin{cases} V_{\mathrm{LJ}}(r_{ij}) & r_{ij} \leqslant \sigma \\ V_{\mathrm{LJ}}(r_{ij})\, V_{\mathrm{ang}}(\mathbf{r}_{ij}, \mathbf{p}_{i\alpha}, \mathbf{p}_{j\beta}) & \sigma < r_{ij}. \end{cases} \tag{3}$$

In an effort to avoid unphysical effects, caused by the interaction of patches belonging to two different particles that are separated by a third particle located in between them, the potential has been truncated at $r_c = 1.9\sigma$.

At this point we emphasize that this potential should rather be considered as a simplistic model potential than as a realistic interaction for patchy colloidal systems. Its main defect becomes evident as we consider the two arrangements of particles shown in figure 2: based on the above interaction, these configurations are characterized by the same energy but, considered as a particle arrangement in a realistic system, they are definitely not equivalent.

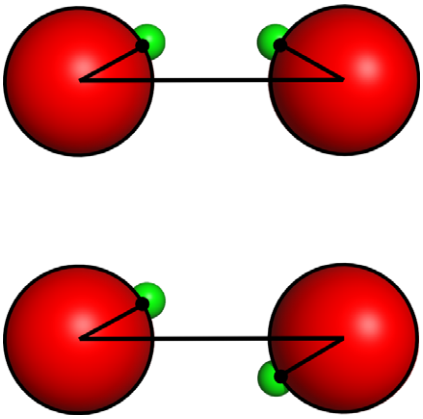

Figure 2. Two configurations of patchy particles that are characterized by the same energy (based on the interparticle potential defined in equations (1)–(3)), but represent inequivalent particle arrangements (see text).

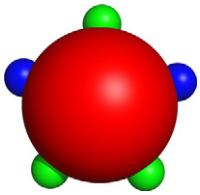

Figure 3. Five-patch particle, decorated with two A and three B patches; in this model like patches attract each other, while unlike patches repel each other (see text).

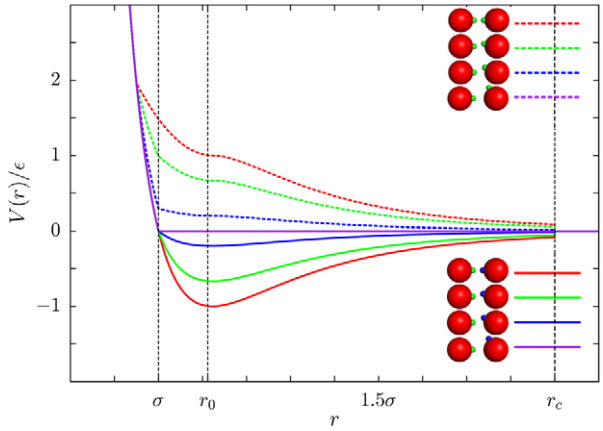

Figure 4. Repulsive and attractive potentials between like and unlike patches for the patchy particle, schematically represented in figure 3. The explicit expressions for these interactions are given in equations (1)–(4). Symbols: dotted lines—repulsion between like patches, full lines—attraction between unlike patches. The potentials are displayed (from top to bottom for the repulsion and from bottom to top for the attraction) for the following angles Θ: 0 (red), 0.2 (green), 0.4 (blue) and 1 (purple). The corresponding particle configurations are displayed schematically.

Further, we have also considered attraction and repulsion between the patches: in this model the particles are decorated by two different types of patches, denoted by indices A or B (cf figure 3). Interactions between different kinds of patches are considered to be attractive and their potential is given by equations (1)–(3). The interaction between like patches are assumed to be repulsive; they are modelled in the following way:

$$V_{\mathrm{II}}(\mathbf{r}_{ij}, \mathbf{p}_{i\alpha}, \mathbf{p}_{j\beta}) = \begin{cases} V(\mathbf{r}_{ij}, \mathbf{p}_{i\alpha}, \mathbf{p}_{j\beta}) & r_{ij} \leqslant r_1 \\ V_{\mathrm{LJ}}(r_{ij}) + [V_1(r) - V_{\mathrm{LJ}}(r)] & \\ \quad \times V_{\mathrm{ang}}(\mathbf{r}_{ij}, \mathbf{p}_{i\alpha}, \mathbf{p}_{j\beta}) & r_1 < r_{ij} \leqslant \sigma \\ V_1(r) V_{\mathrm{ang}}(\mathbf{r}_{ij}, \mathbf{p}_{i\alpha}, \mathbf{p}_{j\beta}) & \sigma < r_{ij} \leqslant r_0 \\ -V(\mathbf{r}_{ij}, \mathbf{p}_{i\alpha}, \mathbf{p}_{j\beta}) & r_0 < r_{ij}, \end{cases} \quad (4)$$

with $I = A$ or B; further, $r_1 = 0.95\sigma$ and $r_0 = \sqrt[6]{2}\sigma$. The potential $V_1(r)$ is quadratic in r and chosen in such a way that

$$V_1(r_1) = V_{\mathrm{LJ}}(r_1) \qquad V_1(r_0) = -V_{\mathrm{LJ}}(r_0) = 1. \quad (5)$$

$V_{\mathrm{II}}(\mathbf{r}_{ij}, \mathbf{p}_{i\alpha}, \mathbf{p}_{j\beta})$ is depicted in figure 4.

2.2. Theoretical tools

As an optimization technique, we use an approach that is based on ideas of GAs. In this concept the different ordered particle arrangements are considered as individuals $\mathcal{I}$ and are exposed to an artificial evolution on the computer. In this evolution they can only 'survive' if the respective thermodynamic potential becomes as small as possible.

To be more specific, we have implemented a phenotype version of the GA-based optimization tool, as it has, for instance, been used in earlier work [67–71]. In this approach, global optimization is achieved by performing GA steps, which ideally transfer the system to promising regions of the potential energy surface in combination with local optimization steps, which relax the system to local minima on this surface. In more detail, this method works as follows: a number of ordered (test) configurations, each corresponding to an individual $\mathcal{I}$, is created in a random fashion, where the parameters that specify an individual are the Cartesian components of the lattice vectors and the coordinates of the basis particles, whose number is externally fixed. All these individuals are relaxed to local minima using an implementation of the Broyden–Fletcher–Goldfarb–Shanno method (L-BFGS-B) [72, 73], i.e. an efficient quasi-Newton algorithm for large-scale optimization problems. Then, a fitness value is assigned to each individual, which is the larger the lower the thermodynamic potential, which characterizes the system, is; since we work in the NPT ensemble, the related thermodynamic potential is the Gibbs free energy G.

The subsequent steps represent the main GA loop: a new set of individuals (which we term generation) is created by (i) copying a certain number of energetically most favourable configurations from the previous generation, (ii) recombining individuals and (iii) mutating individuals. The latter two operations can be briefly described as follows: (ii) for the recombination operation, two individuals, $\mathcal{I}_a$ and $\mathcal{I}_b$, from a given generation are randomly selected, with a selection probability depending on their respective fitness values. The structures that correspond to these individuals are both cut by a

line which is defined via two randomly chosen lattice vectors. From these structural pieces a new test configuration is created, consisting of n particles of individual $\mathcal{I}_a$, located on one side of this line, and $(n - n_b)$ particles of individual $\mathcal{I}_b$ being located on the other side of the line; here n_b is the number of basis particles and n is an integer random number, with $0 \leqslant n \leqslant n_b$. The lattice vectors of the new individual are determined as randomly weighted averages of the lattice vectors of $\mathcal{I}_a$ and $\mathcal{I}_b$. (iii) Mutation of an individual is carried out by multiplying its lattice vectors with a random, symmetric strain matrix as specified in [71].

All these new individuals, created either by recombination or by mutation, are locally optimized with the L-BFGS-B method. Together with the individuals kept from the previous generation they now form the subsequent generation. In the last part of the main GA loop, it is ensured that the new generation fulfills certain conditions. These are: (i) hard constraints for all individuals, i.e. a minimum value for the angle α between the lattice vectors of an individual is imposed, and (ii) niche conditions, i.e. all individuals are required to have a minimum difference δG in their Gibbs free energy values and furthermore the number of individuals with the same α value is limited. The hard constraints guarantee that unphysical regions of the parameter space are excluded, while the niche conditions should maintain diversity in the population, preventing thus a premature convergence to local minima. Any individuals not fulfilling these conditions are discarded and replaced by newly created ones; of course, these have to fulfil the above conditions, as well. For a more detailed presentation of phenotype implementations of GA-based optimization tools we refer to [67–71].

After creating a sufficiently large number of generations, the GA iteration is terminated and the individual with the overall lowest thermodynamic potential is stored and considered as the solution of the GA run. Usually ten independent runs of the algorithm are performed for a given state point and the results are checked for consistency.

In order to be sure that, for a given state point, the 'true' global minimum has indeed been identified, we run in addition GA-search runs assuming up to 20 basis particles per unit cell. These additional runs are also very helpful to check the internal consistency of the data, since any lattice with n_b basis particles can be describe in a different, but equivalent, parametrization, using $m \cdot n_b$ basis particles, m being some arbitrary integer.

3. Results

Our investigations were carried out at constant pressure P; thus the Gibbs free energy, G, has to be minimized. At $T = 0$, G reduces to

$$G = U + PA, \tag{6}$$

U being the internal energy, i.e. the lattice sum, and A being the area of the system. Introducing the following reduced, dimensionless units, $G^\star = G/N\epsilon$, $U^\star = U/N\epsilon$ and $P^\star = P\sigma^2/\epsilon$, the above relation is

$$G^\star = U^\star + P^\star/(\eta\sigma^2) \tag{7}$$

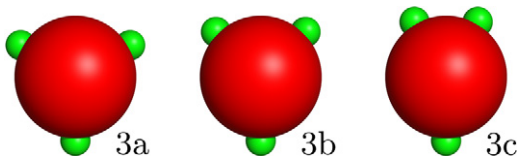

Figure 5. Three-patch particles with three different decorations as they are investigated in the present study: left panel—type 3a, regular patch distribution, i.e. with a set of inter-patch angles of {120°, 120°, 120°}, centre panel—type 3b, with a set of inter-patch angles of {90°, 135°, 135°}, and right panel—type 3c, with a set of inter-patch angles of {60°, 150°, 150°}.

where $\eta = A/N$ is the area number density and N is the number of particles.

We emphasize that for this particular choice of ensemble the pressure is imposed at a given state point. The search algorithm returns the optimal lattice as well as the (area) number density, η.

The following different classes of patchy systems have been considered:

(a) a one-component system of patchy particles with attractive patch–patch interactions (cf equations (1)–(3)), where different decorations of the particles with patches have been considered;
(b) a binary mixture of patchy particles with attractive patch–patch interactions (cf equations (1)–(3)); the two different species are specified by their number of patches;
(c) a one-component system of patchy particles where the patches display both attractive as well as repulsive interactions (cf equation (1)–(4)).

In the following we discuss the MECs of these systems.

3.1. One-component system with attractive patch–patch interactions

Three-patch particles. We have considered three different decorations of the colloidal particles with patches: they are schematically depicted in figure 5 and will be denoted by types 3a, 3b and 3c, respectively. The MECs that we could identify for these three types of patchy particles are summarized in figure 6. While the patchy particles of types 3a and 3c display only two different MECs, type 3b particles form in total four different MECs over the investigated pressure range.

At low pressure all patches are saturated via bonds, forming thereby hexagons. These ring-like structures are regular for particle type 3a and represent the basic units for the honeycomb structure. The hexagons become more elongated as we increase the asymmetry in the patch decoration. At the high-pressure side, the system minimizes its Gibbs free energy rather via the area term, while the number of bonds that the particles are able to form via the patches plays a rather minor role in these energetic considerations. Thus, at high pressure the system forms hexagonal structures where the cores of the particles are close-packed.

For the patchy particles of types 3a and 3c these two phases are the only ones that emerge over the entire pressure range. For the particles of type 3b two additional, intermediate

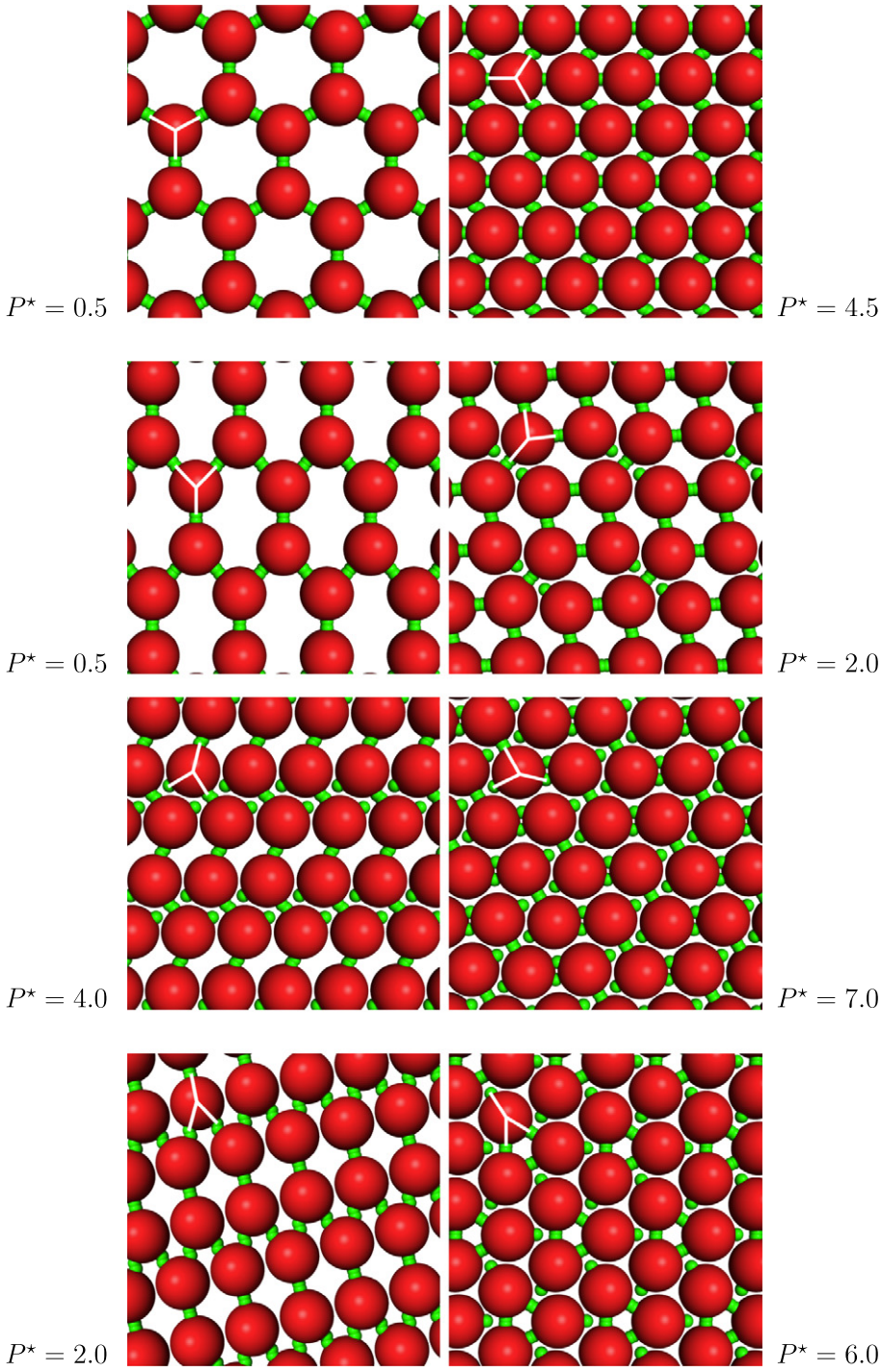

Figure 6. MECs of a one-component system where particles are decorated with three attractive patches. Panels in top row—type 3a; panels in rows two and three—type 3b; panels in bottom row—type 3c. The respective particle decorations are highlighted by white bars for a selected particle in each panel.

structures could be identified, which provide some deeper insight into the system's strategy to find the optimum balance between the two contributions to the Gibbs free energy, according to equation (6): as the pressure is increased, some of the bonds of the low-pressure phase are broken, but the system still tries to maintain as many bonds as possible, forming thereby square or, with increasing pressure, zig-zag lanes. These formations eventually break up to dimers in the high-pressure phase.

In figure 7, we show the reduced Gibbs free energy, $G^\star$, and its contributions according to equation (7) as functions of $P^\star$, for particle types 3a, 3b and 3c. In each case, we focus on the pressure region, where transitions take place. These discontinuous transitions mark the changes between the different MECs depicted in figure 6. Similar behaviour of the Gibbs free energy and its contributions can be observed for the systems discussed in the following paragraphs.

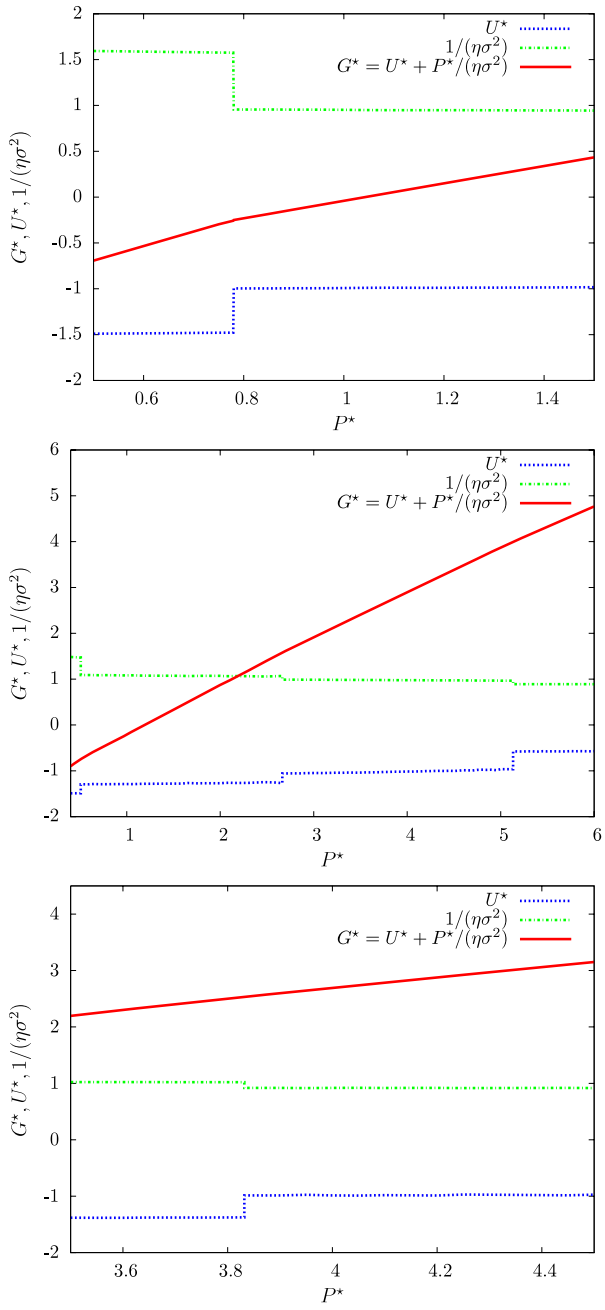

Figure 7. Reduced, dimensionless Gibbs free energy, $G^\star$, and its contributions, $U^\star$ and $1/(\eta\sigma^2)$, according to equation (7), as functions of $P^\star$ for three-patch particles; for symbols, cf legend. From top to bottom—types 3a, 3b and 3c.

Four-patch particles. Again we have considered three types of patch decorations, denoted by type 4a, 4b and 4c; they are schematically depicted in figure 8. In all cases we observe only two MECs over the entire pressure range, i.e. a low- and a high-pressure configuration; they are all depicted in figure 9. The former one is imposed by the requirement that all patches are saturated, which for all three types of decoration is indeed possible. The structure itself is a direct consequence of the particular patch decoration, i.e. the inter-patch angles can easily be identified as the angles between the lattice vectors. In the high-pressure phases, on the other hand, we recover the

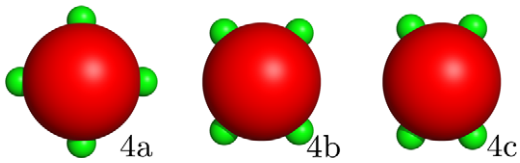

Figure 8. Four-patch particles with three different decorations as they are investigated in the present study: left panel—type 4a, regular patch distribution, i.e. with a set of inter-patch angles of {90°, 90°, 90°, 90°}, centre panel—type 4b, with a set of inter-patch angles of {75°, 105°, 75°, 105°} and right panel—type 4c, with a set of inter-patch angles of {60°, 120°, 60°, 120°}.

hexagonally close-packed lattice where an optimized packing of the particles is energetically more relevant than saturating the patches via bonds. As a consequence, in general some of the patches remain unsaturated. The fact that, for the type 4c particles, all patches are bonded in the high-pressure phase is imposed by the particular choice of inter-patch angle and is thus a fortuitous coincidence.

Five-patch particles. Dealing with five-patch particles offers the possibility of a direct comparison with the results presented in [44]; the MECs identified for $w = 2\pi \cdot 0.05$ are displayed in figure 10. At low pressure we encounter, as in [44], the so-called σ-phase; as the pressure is increased, we observe an intermediate phase which then, at high pressure, becomes a hexagonal particle arrangement. These findings are in good agreement with the results displayed in figure 6 of [44].

Variation of patch width. Investigations with variable patch width reveal some additional interesting features. We present results for the four- and five-patch particles, assuming a regular particle decoration. For the four-patch case we have considered two different w values, namely $w = 2\pi \cdot 0.05$ (representing a well-focused patch) and $w = 2\pi \cdot 0.13$, i.e. a rather extended patch. Working at intermediate pressure we recover two different MECs, displayed in figure 11: for the former case we identify a square lattice where all patches are saturated. For $w = 2\pi \cdot 0.13$, on the other hand, the larger patch width allows for less-focused bonding, thus offering the system a better packing of the particles which results in a close-packed structure.

As we proceed to the five-patch case, we are again able to compare with results presented in [44]. Working at intermediate pressure, we have considered two w values, namely $w = 2\pi \cdot 0.03$ and $w = 2\pi \cdot 0.05$ (cf figure 12); in the nomenclature of Doye *et al* they correspond to the H and σ phases. Again, the more focused patches lead to rather open structures while for the case of more extended patches, the particles are in closer contact. On this occasion we point out that our MECs encountered for $w = 2\pi \cdot 0.03$ differ slightly from the H phase predicted in [44] for this system. In an effort to specify these differences we have depicted the bottom row of figure 12 as the different tilings of two-dimensional space by the distorted hexagonal tiles. Our MEC is built up by hexagons of alternating orientation, while in the H phase of [44], these hexagonal tiles are arranged in a parallel way, where the tiles of the former configuration have a slightly smaller area. A closer investigation of the $G^\star$ values of the two configurations reveals

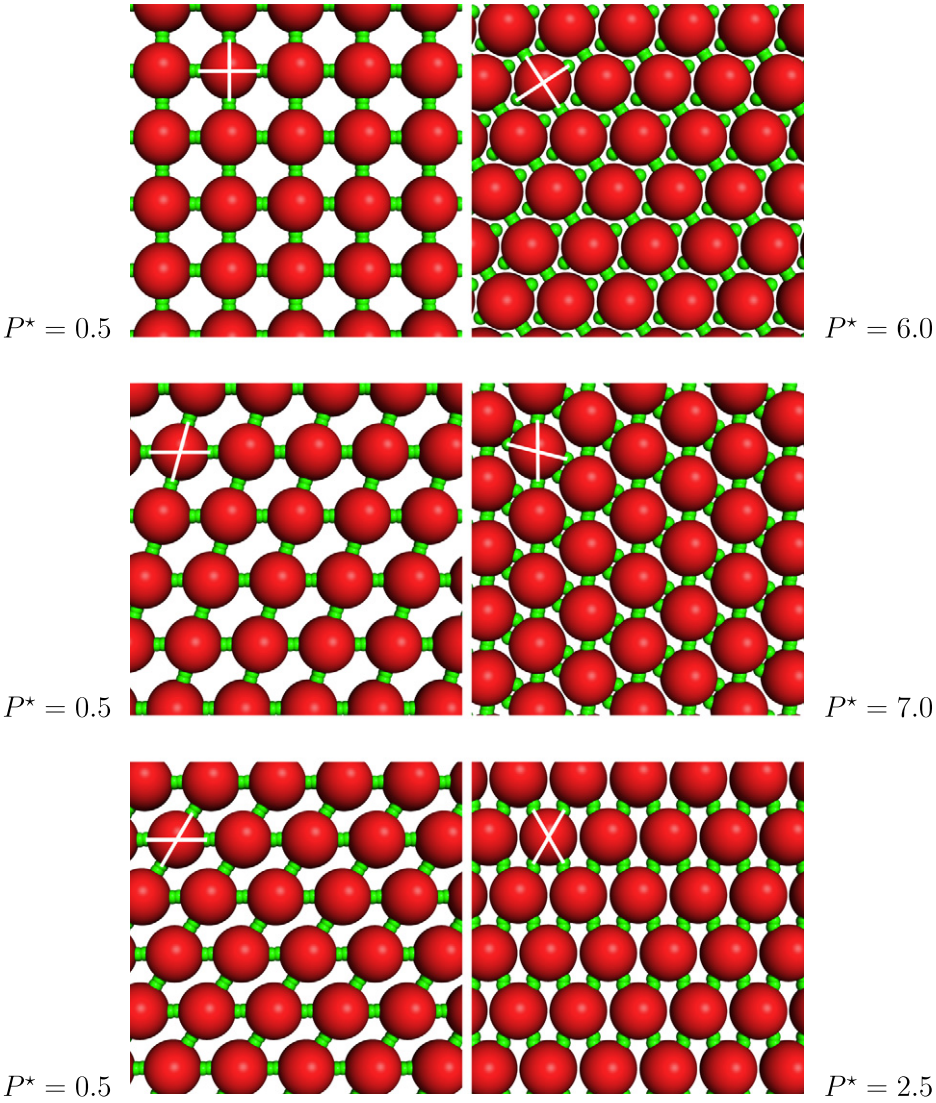

Figure 9. MECs of a one-component system where particles are decorated with four attractive patches. Panels in top row—type 4a; panels in second row—type 4b; panels in bottom row—type 4c. The respective particle decorations are highlighted by white bars for a selected particle in each panel.

a minute difference in energy: −0.200 18 versus −0.200 66. At $P^\star = 1$, it is mainly the area-dependent contribution of G that favours our configuration, while the difference in the potential energy $U^\star$ is smaller by a factor of five. These findings nicely confirm the power of GAs as a highly sensitive optimization tool that is able to decide between competing structures of minute energy differences.

3.2. Mixtures

We have considered an equimolar, binary mixture of patchy particles composed by two- and three-patch particles with a regular decoration and the standard value for the patch width, w.

Similar to the investigations on the one-component system we observe that at low pressure the MECs are triggered by the request to saturate as many patch bonds as possible. As the pressure is increased, this requirement is gradually released and the self-assembly strategy is based on a compromise between bond formation and packing. Finally, in the high-pressure phase we recover the hexagonal particle arrangement. In figure 13 we display the three self-assembly scenarios identified for this binary mixture.

3.3. Patchy particles with attractive and repulsive patches

Since for this system the number of parameters that can be varied is fairly large, we restrict ourselves to a particular system: our particles are decorated by five patches (cf figure 3) where two of them are of type A, while the other three are of type B. From our investigations we have evidence that this lack of parity induces considerably more interesting self-assembly scenarios than those encountered in systems where the numbers of A and B patches are equal.

By varying the pressure we could identify four different MECs, depicted in figure 14. At low pressure, we observe

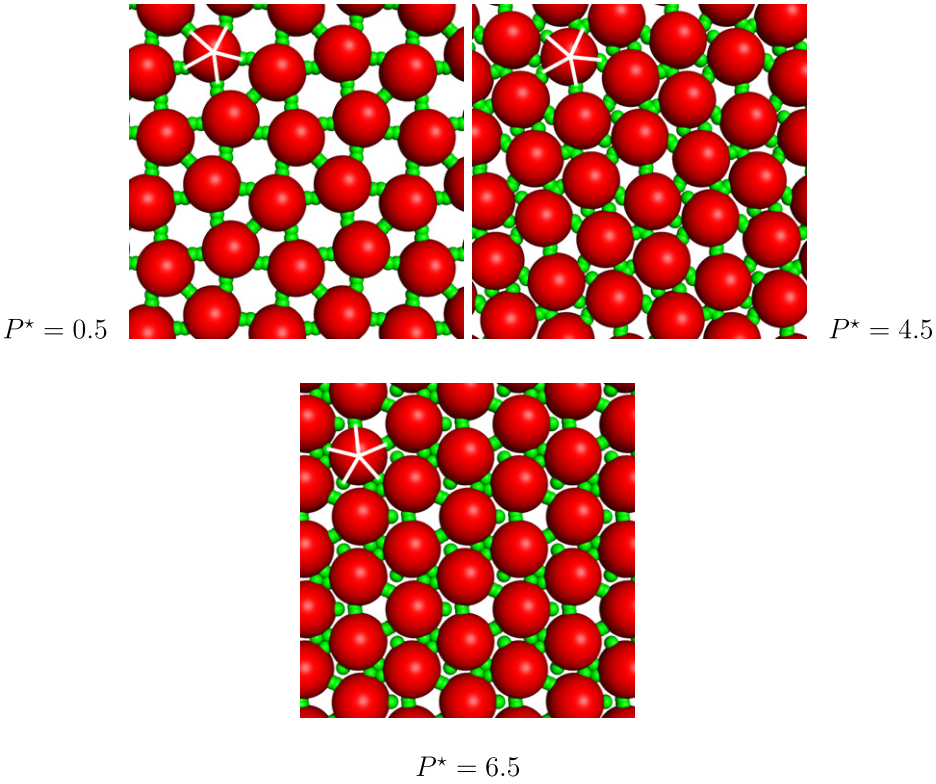

Figure 10. MECs of a one-component system where particles are decorated with five attractive patches. The respective particle decorations are highlighted by white bars for a selected particle in each panel.

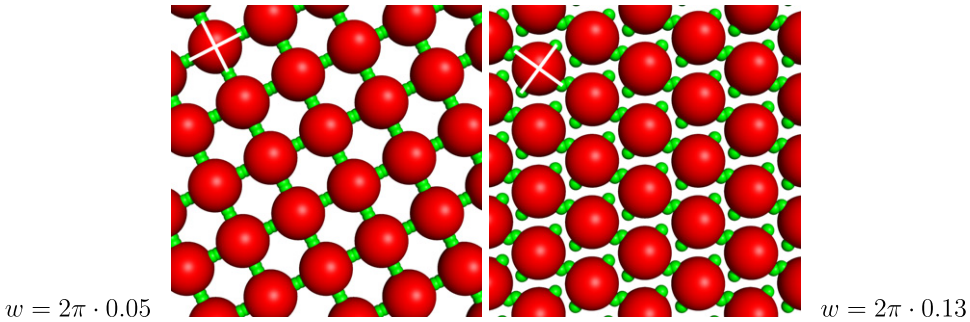

Figure 11. MECs of a one-component system where particles are decorated with four attractive patches with different w parameters ($P^\star = 1$). The respective particle decorations are highlighted by white bars for a selected particle in each panel.

a tiling of the two-dimensional space by triangular-shaped, equilateral units (see highlighted tiles in figure 14), that consist of six particles, with all tiles pointing in the same direction. Note that all A patches are saturated by a B patch, so that only one B patch per particle remains unbound, which points towards the centre of the triangular unit. As the pressure is increased, the system forms elongated, closed structures, composed of six particles which now cover in alternating orientation the two-dimensional space (see again highlighted tiles in figure 14). Still, almost all A–B bonds are saturated, but the increased pressure forces the (mutually repulsive) B patches to approach each other. Finally, at the highest pressure, we observe hexagonal particle arrangements. At first sight, the system seems to be isotropic. However, one easily observes a substructure, characterized by the orientation of the particles. The system forms double lanes: using the terminology introduced for the bonds in figure 15, adjacent pairs of lanes are stabilized via the strong B1 bonds, while inside each pair of lanes we observe B2 and B3 bonds, both of them being energetically less favourable. In a closer analysis of the energies of these bonds one recovers the following U/ϵ values: $U_{B1}/\epsilon = -0.75$, $U_{B2}/\epsilon = -0.13$ and $U_{B3}/\epsilon = -0.06$. The strength of the B1 bond can be easily traced back to the small angles involved, while the weakness of the B3 bond is due to the large distances between the patches.

4. Conclusion and outlook

This contribution deals with the first application of GA-based optimization tools to identify ordered configurations

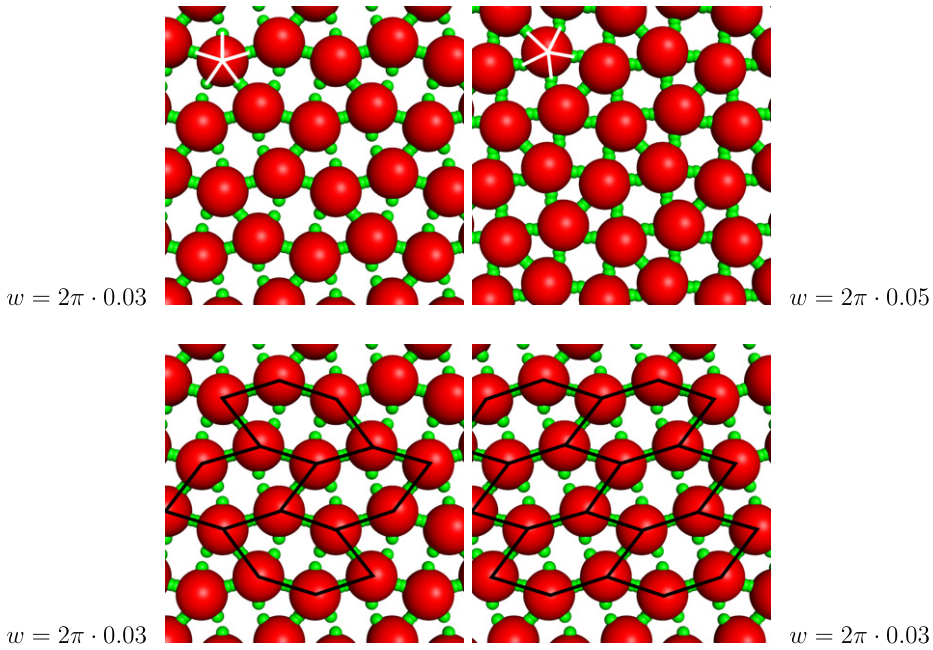

Figure 12. MECs of a one-component system where particles are decorated with five attractive patches with different w parameters ($P^\star = 1$). Top row: results from the present work, where the MEC in the right panel corresponds to the σ phase of [44]. Bottom row: comparison of results for $w = 2\pi \cdot 0.03$; left—same MEC as in the top left panel, with highlighted tiling; right—MEC as predicted in [44] (so-called H phase), with highlighted tiling.

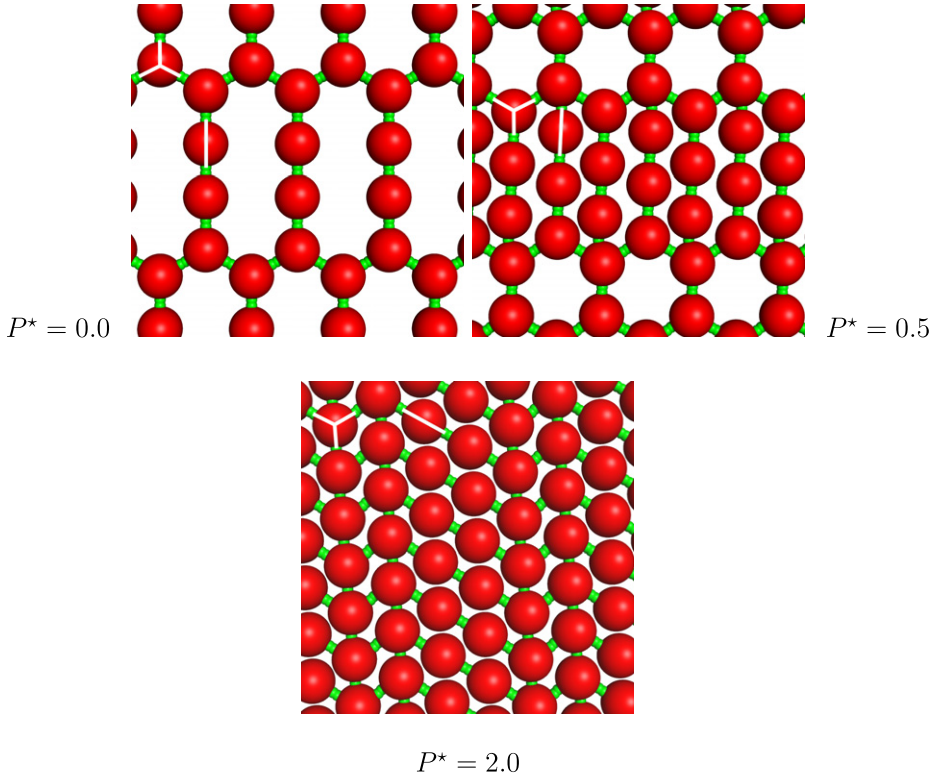

Figure 13. MECs for an equimolar, binary mixture of patchy particles, decorated with two and three patches, assuming a regular patch decoration. The respective particle decorations are highlighted by white bars for two selected particles in each panel.

of patchy particles. Due to the fact that for directional potentials the numerical effort of this approach is considerably enhanced with respect to particles with spherically symmetric interactions, we have restricted ourselves to a simple model: we work in two dimensions and use particle and patch interactions that are based on potentials proposed recently in the literature [44].

From the methodological point of view, our investigations are yet another demonstration that GA-based optimization techniques represent a very attractive tool to identify ordered

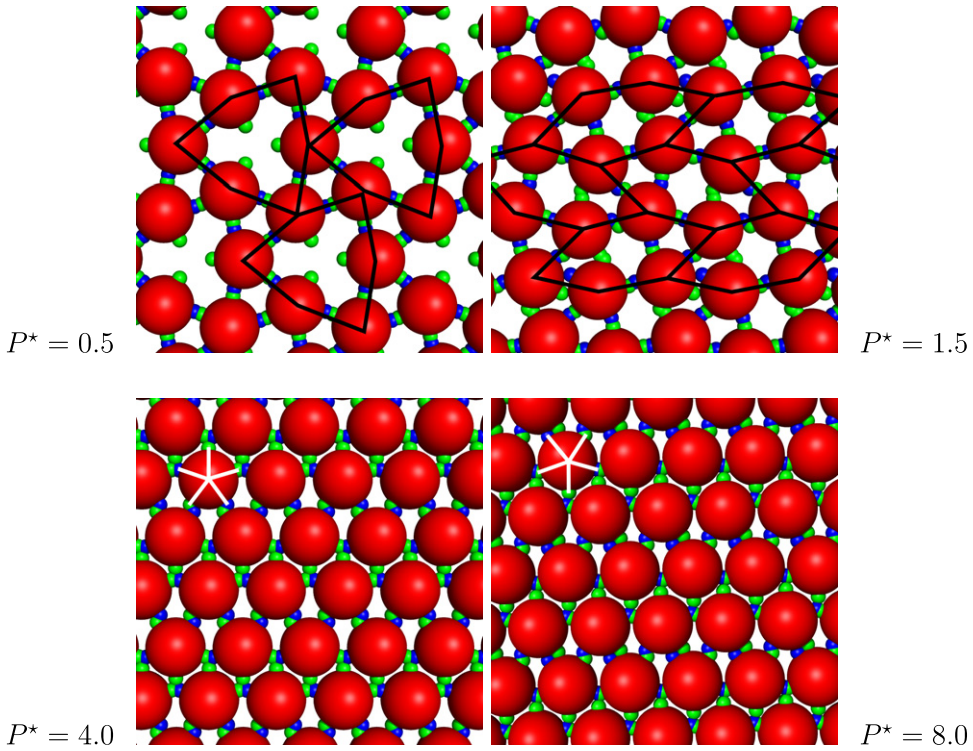

Figure 14. MECs of patchy particles, decorated by two A and three B patches (cf section 2.1 and figure 3).

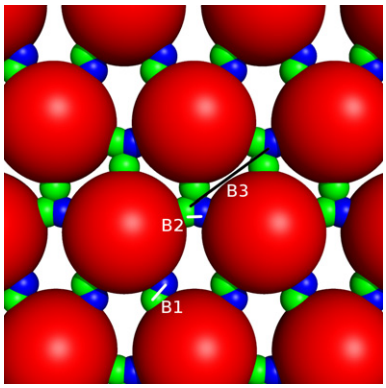

Figure 15. Left panel of bottom row of 14, highlighting the bonds that are discussed in the text.

equilibrium structures in (soft) condensed matter systems: (i) this numerical tool is highly efficient and reliable, it copes extremely well with rugged energy landscapes and high-dimensional search spaces—we were able to include up to 20 basis particles in our unit cells. (ii) Furthermore, GA-based optimization techniques represent very sensitive antennas to discriminate between competing structures that differ in energy only by a minute amount, i.e. one-tenth of a per cent or even less.

Concerning the structural properties of two-dimensional patchy particle systems, we could identify a broad variety of ordered equilibrium structures; the parameters that turn out to be responsible for these self-assembly scenarios are: the number of patches and their interactions, the patch decorations and, of course, the external parameters, such as the pressure or the composition of the system. Working in the NPT ensemble, we could filter out the following strategies for self-assembly: at low pressure, the systems try to saturate as many patch bonds as possible, leading to rather open structures. At high pressure, on the other hand, particles arrange in close-packed hexagonal structures; now the saturation of bonds plays a minor role with respect to the effects to pack particles as efficiently as possible and to minimize in this way the volume (i.e., area) contribution to the Gibbs free energy. Although isotropic at first sight, these close-packed particle arrangements display a rich internal structure. They can be classified by the bonding behaviour between the particles: in our MECs we were able to identify lanes of different shapes, rings, dimers or trimers. In the intermediate pressure range, the ordered particle configurations are imposed by energy minimization, which is a trade-off between the energetic contribution (i.e. via bonding) and the volume/area part (i.e. via packing).

The most obvious extension of the present work aims, of course, at investigations of self-assembly scenarios of patchy particles in *three* dimensions. However, this generalization brings along a considerably enhanced conceptual and numerical complexity. On one side, already in two dimensions, the treatment of orientational interactions leads to an increase in the dimensionality of the search space compared to spherically symmetric potentials. This effect has an even larger impact in three dimensions. On the other side, the additional degrees of freedom considerably raise the numerical costs for the evaluation of the lattice sum (and of its derivatives); a recently developed framework for efficient calculation of derivatives of orientational interactions in three

dimensions [74] will certainly be very helpful to reduce these computational expenses.

Another challenging extension of GA-based optimization techniques in soft matter physics is to proceed to finite temperatures, requiring thus the inclusion of entropic contributions to the thermodynamic potentials. In principle, the thermodynamic properties of the MECs can be evaluated even at finite temperatures with suitable concepts, such as classical density functional theory [75]. However, while at $T = 0$ the evaluation of the thermodynamic potential reduces essentially to the calculation of the lattice sums (which can be done within machine precision), the approximate character of the finite temperature frameworks introduces some conceptual uncertainty in the numerical results whose consequences are difficult to grasp. These can be of particular relevance, when competing structures are characterized by minute energy differences.

Acknowledgments

The authors are indebted to Julia Fornleitner (Wien) for stimulating discussions and for computational aid. EB acknowledges financial support from the Erwin Schrödinger International Institute for Mathematical Physics (ESI) within an ESI Junior Research Fellowship. Further, financial support by the Austrian Science Foundation (FWF) under project no. W004 is gratefully acknowledged.

References

[1] Lu Y, Yin Y and Xia Y 2001 *Adv. Mater.* **13** 415
[2] Liddell C M and Summers C J 2003 *Adv. Mater.* **15** 1715
[3] Manoharan V N, Elsesser M T and Pine D J 2003 *Science* **301** 483
[4] Cho Y S, Yi G R, Lim J M, Kim S H, Manoharan V N, Pine D J and Yang S M 2005 *J. Am. Chem. Soc.* **127** 15968
[5] Zerrouki D, Rotenberg B, Abramson S, Baudry J, Goubault C, Leal-Calderon F, Pine D J and Bibette J 2006 *Langmuir* **22** 57
[6] Mirkin C A, Letsinger R L, Mucic R C and Storhoff J J 1996 *Nature* **382** 607
[7] Geerts N, Schmatko T and Eiser E 2008 *Langmuir* **9** 5118
[8] Schmatko T, Bozorgui B, Geerts N, Frenkel D, Eiser E and Poon W C K 2007 *Soft Matter* **3** 703
[9] Banerjee I A, Yu L T and Matsui H 2003 *Nano Lett.* **3** 283
[10] Fraenkel-Conrat H and Williams R C 1955 *Proc. Natl Acad. Sci. USA* **41** 690698
[11] Nguyen H D, Reddy V S and Brooks C L III 2007 *Nano Lett.* **7** 338
[12] Van Workum K and Douglas J F 2006 *Phys. Rev.* E **73** 031502
[13] Hiddessen A L, Rotgers S D, Weitz D A and Hammer D A 2000 *Langmuir* **16** 9744
[14] Hiddessen A L, Weitz D A and Hammer D A 2004 *Langmuir* **20** 71
[15] Glotzer S C 2004 *Science* **306** 419
[16] Glotzer S C and Solomon M J 2007 *Nat. Mater.* **6** 557
[17] Zhang Z L and Glotzer S C 2004 *Nano Lett.* **4** 1407
[18] Wilber A W, Doye J P K, Louis A A, Noya E G, Miller M A and Wong P 2007 *J. Chem. Phys.* **127** 085106
[19] Wertheim M S 1984 *J. Stat. Phys.* **35** 19
[20] Wertheim M S 1984 *J. Stat. Phys.* **35** 35
[21] Wertheim M S 1986 *J. Stat. Phys.* **42** 459
[22] Wertheim M S 1986 *J. Stat. Phys.* **42** 477
[23] Kolafa J and Nezbeda I 1987 *Mol. Phys.* **61** 161
[24] Sear R P 1999 *J. Chem. Phys.* **111** 4800
[25] Sear R P 2006 *Curr. Opin. Colloid Interface Sci.* **11** 35
[26] Busch N A, Wertheim M S and Yarmush M L 1996 *J. Chem. Phys.* **104** 3962
[27] Sear R P and Jackson J G 1996 *J. Chem. Phys.* **105** 1113
[28] Kern N and Frenkel D 2003 *J. Chem. Phys.* **118** 9882
[29] Trappe V and Sandkühler P 2004 *Curr. Opin. Colloid Interface Sci.* **8** 494
[30] Cipelletti L and Ramos L 2005 *J. Phys.: Condens. Matter* **17** R253
[31] Zaccarelli E 2007 *J. Phys.: Condens. Matter* **19** 323101
[32] Sciortino F and Tartaglia P 2005 *Adv. Phys.* **54** 471
[33] Sciortino F, Buldyrev S, De Michele C, Ghofraniha N, La Nave E, Moreno A, Mossa S, Tartaglia P and Zaccarelli E 2005 *Comput. Phys. Commun.* **169** 166
[34] Tartaglia P and Sciortino F 2010 *J. Phys.: Condens. Matter* **22** 104108
[35] Zaccarelli E, Buldyrev S V, La Nave E, Moreno A J, Saika-Voivod I, Sciortino F and Tartaglia P 2005 *Phys. Rev. Lett.* **94** 218301
[36] Bianchi E, Largo J, Tartaglia P, Zaccarelli E and Sciortino F 2006 *Phys. Rev. Lett.* **97** 168301
[37] Tavares J, Teixeira P and da Gama M T 2009 *Mol. Phys.* **107** 453
[38] Foffi G and Sciortino F 2007 *J. Phys. Chem.* B **111** 9702
[39] Fantoni R, Gazzillo D, Giacometti A, Miller M A and Pastore G 2007 *J. Chem. Phys.* **127** 234507
[40] Sciortino F 2008 *Eur. Phys. J.* B **64** 505
[41] Huisman B A H, Bolhuis P G and Fasolino A 2008 *Phys. Rev. Lett.* **100** 188301
[42] Sciortino F, Bianchi E, Douglas J F and Tartaglia P 2007 *J. Chem. Phys.* **126** 194903
[43] Bianchi E, Tartaglia P, La Nave E and Sciortino F 2007 *J. Phys. Chem.* B **111** 11765
[44] Doye J P K, Louis A A, Lin I C, Allen L R, Noya E G, Wilber A W, Kok H C and Lyus R 2007 *Phys. Chem. Chem. Phys.* **9** 2197
[45] Noya E G, Vega C, Doye J P K and Louis A A 2007 *J. Chem. Phys.* **127** 054501
[46] Villar G, Wilber A W, Williamson A J, Thiara P, Doye J P K, Louis A A, Jochum M N, Lewis A C and Levy E D 2009 *Phys. Rev. Lett.* **102** 118106
[47] Jankowski E and Glotzer S C 2009 *J. Chem. Phys.* **131** 104104
[48] Stucke D P and Crespi V H 2003 *Nano Lett.* **3** 1183
[49] Gottwald D, Likos C N, Kahl G and Löwen H 2004 *Phys. Rev. Lett.* **92** 068301
[50] Gottwald D, Likos C N, Kahl G and Löwen H 2005 *J. Chem. Phys.* **122** 074903
[51] Mladek B M, Gottwald D, Kahl G, Neumann M and Likos C N 2006 *Phys. Rev. Lett.* **96** 045701
[52] Likos C N, Mladek B M, Gottwald D and Kahl G 2007 *J. Chem. Phys.* **126** 224502
[53] Mladek B, Gottwald D, Likos C N and Kahl G 2007 *J. Phys. Chem.* **111** 12799
[54] Pauschenwein G J and Kahl G 2008 *Soft Matter* **4** 1396
[55] Pauschenwein G J and Kahl G 2008 *J. Chem. Phys.* **129** 174107
[56] Fornleitner J, Lo Verso F, Kahl G and Likos C N 2008 *Soft Matter* **4** 480
[57] Dobnikar J, Fornleitner J and Kahl G 2008 *J. Phys.: Condens. Matter* **20** 494245
[58] Filion L and Dijkstra M 2009 *Phys. Rev.* E **79** 046714
[59] Tückmantel T, Lo Verso F and Likos C N 2009 *Mol. Phys.* **107** 523
[60] Chremos A and Likos C N 2009 *J. Phys. Chem.* B **113** 12316
[61] Kahn M, Weis J J, Likos C N and Kahl G 2009 *Soft Matter* **5** 2852
[62] Fornleitner J, Lo Verso F, Kahl G and Likos C N 2009 *Langmuir* **25** 7836

[63] Nikoubashman A and Likos C N 2010 *J. Phys.: Condens. Matter* **22** 104107
[64] Fornleitner J and Kahl G 2010 *J. Phys.: Condens. Matter* **22** 104118
[65] Pauschenwein G J and Kahl G 2009 *J. Phys.: Condens. Matter* **21** 474202
[66] Gottwald D, Kahl G and Likos C N 2005 *J. Chem. Phys.* **122** 204503
[67] Deaven D M and Ho K M 1995 *Phys. Rev. Lett.* **75** 288
[68] Hartke B 1999 *Comput. Chem.* **20** 1752
[69] Johnston R L 2003 *Dalton Trans.* **2003** 4193
[70] Oganov A R and Glass C W 2006 *J. Chem. Phys.* **124** 244704
[71] Glass C W, Oganov A R and Hansen N 2006 *Comput. Phys. Commun.* **175** 713
[72] Byrd R H, Lu P and Nocedal J 1995 *SIAM J. Sci. Comput.* **16** 1190
[73] Zhu C, Byrd R H and Nocedal J 1997 *ACM T. Math. Software* **23** 550
[74] Chakrabarti D and Wales D J 2009 *Phys. Chem. Chem. Phys.* **11** 1970
[75] Evans R 1992 *Fundamentals of Inhomogeneous Fluids* ed D Henderson (New York: Dekker)